THE JOURNAL OF PHYSICAL CHEMISTRY C

Article

pubs.acs.org/JPCC

# Water Deprotonation via Oxo-Bridge Hydroxylation and $^{18}O$-Exchange in Free Tetra-Manganese Oxide Clusters

Sandra M. Lang,[†] Irene Fleischer,[†] Thorsten M. Bernhardt,*[,†] Robert N. Barnett,[‡] and Uzi Landman*[,‡]

[†]Institute of Surface Chemistry and Catalysis, University of Ulm, Albert-Einstein-Allee 47, 89069 Ulm, Germany

[‡]School of Physics, Georgia Institute of Technology, Atlanta, Georgia 30332-0430, United States

Supporting Information

**ABSTRACT:** One of the fundamental biological reactions, the catalytically activated water-splitting, takes place at an inorganic tetra-manganese monocalcium penta-oxygen ($Mn_4CaO_5$) cluster which together with its protein ligands forms the oxygen evolution complex (OEC) of the membrane-bound pigment–protein photosystem II (PSII) of plants, algae, and cyanobacteria. In the first step of a new hierarchical approach to probe fundamental concepts of the water-splitting reactions, we present the gas-phase preparation of an isolated tetra-manganese oxide cluster ion, $Mn_4O_4^+$, as a simplified model of the OEC. Reactivity studies with $D_2{}^{16}O$ and $H_2{}^{18}O$ in a gas-phase ion trap experiment reveal the exchange of the oxygen atoms of the cluster with water oxygen atoms. This provides direct experimental evidence for the ability of $Mn_4O_4^+$ to dissociate water via hydroxylation of the oxo-bridges. The rate of oxygen exchange in the free cluster agrees well with the conversion rate of substrate water to $O_2$ in photosystem II, thus supporting the involvement of bridging oxygen atoms in this process. First-principles spin density functional theory calculations reveal the molecular mechanism of the water deprotonation and oxo-bridge exchange.

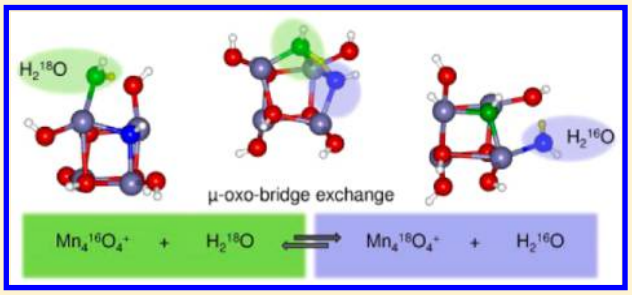




## I. INTRODUCTION

The activation of water and the subsequent evolution of molecular oxygen represent one of the fundamental processes in nature. It is catalyzed by an inorganic core, the tetra-manganese monocalcium penta-oxygen ($Mn_4CaO_5$) cluster, which together with its protein ligands forms the oxygen evolution complex (OEC) of the membrane-bound pigment–protein photosystem II (PSII) of plants, algae, and cyanobacteria.[1] Intensive research efforts in past decades resulted in increasingly precise characterization of the composition and structure of photosystem II. Only recently, high-level X-ray diffraction experiments at 1.9 Å resolution revealed that the OEC consists of a near cubic $Mn_3CaO_4$ unit coordinated to a fourth manganese atom via one of the corner oxygen atoms and an additional fifth oxygen atom by a di-$\mu$-oxo-bridge.[2]

The mechanistic details of water activation and O–O bond formation at the OEC are central to understanding the complex processes in photosystem II, and although significant progress has been made in this direction, complete disentanglement of this problem has not yet been achieved.[3−5] Various mechanisms involving oxygen moieties that are terminally coordinated to, or bridging between, the metal centers of the OEC have been proposed.[5] The most refined recent structural data show, however, that the OEC contains highly stabilized oxo-bridges between three ($\mu_3$) or even four ($\mu_4$) metal atoms, which appears to disfavor O–O bond formation between bridging oxygens.[2,5] Nevertheless, at present, the most elaborate theoretical mechanistic model for water activation and oxidation at the OEC does involve O–O bond formation between bridging oxygens.[5−7]

Through the use of time-resolved membrane inlet mass spectrometry, it has been possible to distinguish between the two water molecules required for the formation of molecular oxygen at the OEC by measurement of their $^{18}O$-exchange rates.[8−11] On the basis of these data in conjunction with Ca/Sr substitution[12] and NMR[13] experiments, a consistent mechanistic model for the water activation and $O_2$ formation emerges in which a fast exchanging water molecule is incorporated at a terminal position bound to a Mn atom in the OEC, whereas a second water replaces a $\mu_3$-oxo-bridge between three metal centers, after dioxygen formation, with an at least 1 order of magnitude slower exchange rate.[11]

The assignment of the slowly exchanging substrate water to a $\mu$-oxo-bridge in the OEC has, however, been challenged by kinetic studies with ligated di-, tri-, and tetra-manganese oxide as well as calcium–manganese oxide complexes.[3,14−18] All of these model-type systems contain exclusively $\mu$-oxo-bridges that exhibit exchange rates which are several orders of magnitude slower than those measured for the OEC.[11]

**Special Issue:** Current Trends in Clusters and Nanoparticles Conference

**Received:** October 23, 2014
**Revised:** December 17, 2014
**Published:** January 5, 2015




DOI: 10.1021/jp5106532
J. Phys. Chem. C 2015, 119, 10881−10887

Thus, it appears mandatory to develop new models, which on one hand are closely related to the biological OEC and on the other hand are simple enough to provide molecular level insight into the mechanistic and energetic details of the catalytic water-splitting process. The question whether this process involves the oxidative incorporation of water as $\mu$-bridging oxide ligands into manganese oxide cluster structures holds the key to a more comprehensive understanding of the operative mechanism of the OEC.[18]

Toward this goal, an approach is pursued here in which we attempt to hierarchically formulate basic concepts for the construction of the water-splitting system. As a first step in this hierarchical approach we have recently employed nonligated gas-phase manganese oxide clusters as simplified models for gaining molecular level insight into the structure and size-dependent water activation mechanism.[19] For the $Mn_4O_4^+$ cluster, ion trap mass spectrometry experiments revealed the formation of $Mn_4O_4(H_2O)_{4-6}^+$ complexes after the reaction with water. Concurrent first-principles spin density functional theory (SDFT) calculations found that the bare $Mn_4O_4^+$ cluster has a two-dimensional ground-state structure. However, after adsorption of water, e.g., $Mn_4O_4(H_2O)_4^+$, the cluster has been found to transform to a three-dimensional cuboid with $\mu_3$-bridging oxygen atoms, in close similarity to the structure of the inorganic core of the OEC.[19] Furthermore, the calculations predicted this tetra-nuclear manganese oxide cluster to deprotonate adsorbed water molecules via the hydroxylation of the $\mu$-oxo-bridges.[19]

We present the first direct evidence for the dissociation of water molecules via hydroxylation of the oxo-bridges of $Mn_4O_4^+$ through oxygen isotope exchange experiments with $D_2{}^{16}O$ and $H_2{}^{18}O$. It has to be noted that the Mn atom formal oxidation state in the resulting $Mn_4(OH)_8^+$ complex ranges between II and III and is thus lower than that for the Mn atoms of the OEC.[11] Nevertheless, the $^{18}O$-exchange rate in the model $Mn_4O_4^+$ cluster is in a range similar to those determined for the OEC in photosystem II in the different oxidation states of the Kok-cycle. In particular, water exchange in PSII is actually slower in S1 with two Mn(III) than in S2 with only one Mn(III);[11,20] hence, it is orders of magnitude faster than in condensed phase ligated model complex systems. First-principles SDFT simulations reveal the detailed mechanism and energetics of the water deprotonation via $\mu$-oxo-bridge-hydroxylation and the $^{18}O$-exchange reaction.

## II. METHODS

**A. Experimental Methods.** The experimental setup consists of a variable temperature radio frequency octopole ion trap inserted into a low-energy ion beam assembly of two quadrupole mass spectrometers and two ion guides. The general experimental layout is described in detail elsewhere and will be outlined only briefly here.[21]

Ligand-free gas-phase manganese oxide clusters are prepared by sputtering of preoxidized Mn metal targets with high-energy Xe ion beams. This approach allows for the controlled preparation of stoichiometric $(MnO)_n^+$. The cluster ion beam is steered into a helium-filled quadrupole ion guide to collimate and thermalize the hot cluster ions before the tetra-manganese oxide cluster is mass-selected from the beam in an adjacent first quadrupole mass filter. The $Mn_4O_4^+$ ion beam is then transferred via a second quadrupole ion guide into the home-built octopole ion trap, which is prefilled with about 1 Pa of helium and small partial pressures of $D_2O$ or $H_2{}^{18}O$. The absolute pressure inside the ion trap is measured by a Baratron gauge (MKS, Typ 627B) attached to the ion trap via a Teflon tube. The amount of water is determined by the vapor pressure of water in the reservoir recipient at room temperature and is typically $\leq$0.001 Pa. All experiments are performed with the ion trap at 300 K. Thermal equilibration of the clusters inside the ion trap is achieved within a few milliseconds under our experimental conditions[21] while the clusters are stored in the ion trap for a considerably longer time, typically between 0.1 s and several seconds. Thus, full thermalization of the clusters inside the ion trap is assured. After the chosen reaction, i.e., storage time, $t_R$, all ionic reactants, intermediates, and products are extracted from the ion trap and the ion distribution is subsequently analyzed by a second quadrupole mass spectrometer.

**B. Theoretical Methods.** The theoretical explorations of the atomic arrangements and electronic structures of the manganese oxide clusters and their complexes were performed with the use of the Born−Oppenheimer spin density-functional theory molecular dynamics (BO-SDFT-MD) method[22] with norm-conserving soft (scalar relativistic for Mn) pseudopotentials[23] and the generalized gradient approximation (GGA)[24] for electronic exchange and correlations. In these calculations we have used a plane-wave basis with a kinetic energy cutoff ($E_c$) of 62 Ry, which yields convergence. This corresponds to a real-space grid spacing of 0.4 $a_0$ (Bohr radius); the real-space grid spacing for the density (and potential) was 0.133 $a_0$ corresponding to $E_c$ = 555 Ry. In the construction of the Mn pseudopotentials, the valence electrons, $3d^5$ and $4s^2$, were characterized by core radii $r_c(s)$ = 2.35 $a_0$ and $r_c(d)$ = 2.35 $a_0$, with the s orbital treated as local. For the oxygen atom pseudopotential, the valence $2s^2$ and $2p^4$ electrons were treated with $r_c(s) = r_c(p)$ = 1.45 $a_0$, with the p orbital treated as local.

The BO-SDFT-MD method is particularly suitable for investigations of charged systems because it does not employ a supercell (i.e., no periodic replication of the ionic system is used). In all the calculations the dependence on spin multiplicity has been checked, and the results that we report correspond to the spin multiplicities with the lowest energies. In particular, it is pertinent to note here that in all our calculations the spin-degree of freedom is optimized and used in the computation, unless a particular spin configuration (spin multiplicity) is prescribed. At each step of the calculation the energy levels of the SDFT up-spin and down-spin manifolds in the vicinity of the Fermi level are examined, and the occupation is adjusted such that the spin-Kohn−Sham level with the lower-energy eigenvalue gets occupied. From these calculations we determined that for the water exchange process investigated in this work the spin multiplicity of the $Mn_4O_4(D_2O)_n^+$ ($n$ = 4−6) clusters remains unchanged with the spin-projection taking its maximal value, $S_z$ = 19/2 (corresponding to the 19 unpaired d-electrons of the four Mn atoms in the cluster cation); for details and further information about higher-energy spin isomers (e.g., isomers with $S_z$ = 9/2 and 1/2) of the $Mn_4O_4(D_2O)_5^+$ cluster, see Supporting Information.

The energy minimization to find the optimal cluster geometry was done with a steepest-descent method. The convergence criteria was that the maximum force magnitude on any particle is less than 0.0005 hartree/Bohr and that the average over all particles is less than 0.00025 hartree/Bohr. BO-SDF-MD simulations of typically a few picosecond duration at 300 K (that is, canonical, constant temperature simulations with stochastic themalization) were used to ensure that the


DOI: 10.1021/jp5106532
J. Phys. Chem. C 2015, 119, 10881−10887

resulting optimal configurations were stable; a time-step of 0.25 fs was used in these simulations. For the clusters with adsorbed water, longer runs were used to explore configuration space and suggest starting geometries for the minimization. In addition, BO-SDF-MD simulations were used to explore the water-splitting process on the $Mn_4O_4(H_2O)_4^+$ cluster. For completeness, we remark here that although no calculations have been performed to date for the system investigated by us in the present paper (see, however, ref 19), a number of theoretical treatments have been published addressing various aspects of the metal-oxide cluster of the OEC (specifically the $Mn_4CaO_5$ cluster) with amino acid residues and water molecules linked to the core cluster; in addition to several theoretical papers cited already in the introductory section, we note here refs 25−27.

In the first-principles SDFT calculations of the reaction profile shown for $Mn_4O_4(H_2O)_5^+$ in Figure 2, a reaction coordinate was judiciously chosen. In this case the reaction coordinate consists of the ratio of O−H distances, that is, $d(O_W{-}H)/d(O_C{-}H)$, where H is the transferred hydrogen (marked yellow in Figure 2). For each value of the reaction coordinate, the total energy of the system was optimized through unconstrained relaxation of all of the other degrees of freedom of the system; as mentioned previously, the relaxation process includes optimization with respect to the spin degrees of freedom. The reaction profile (reaction path) was obtained via incrementing the reaction coordinate by small steps to find the local minima and barrier configurations. These calculations yield results that are the same as, or close to, those obtained by other methods, e.g., the nudged elastic band and variants thereof; see the discussion on pp 89 and 90 in ref 28.

## III. RESULTS AND DISCUSSION

**A. Water Complexes of Tetra-Manganese Oxide Clusters.** Figure 1a (black line) displays a mass spectrum obtained after the reaction of the tetra-manganese oxide cluster $Mn_4O_4^+$ with $D_2O$ for 0.1 s in the gas-filled ion trap.[19] The cluster reacts fast (faster than the time resolution of the experiment) to form three products, which are shifted by 80, 100, and 120 amu from the position of the bare cluster signal (284 amu). These product peaks can be assigned to the product complexes $Mn_4O_4(D_2O)_4^+$, $Mn_4O_4(D_2O)_5^+$, and $Mn_4O_4(D_2O)_6^+$, respectively, with $Mn_4O_4(D_2O)_5^+$ representing the product with the highest intensity.

The mass spectrum does not change at longer reaction times; thus, the observed reaction products can be considered to be in equilibrium. Consequently, a straightforward reaction mechanism for the sequential adsorption of the first four water molecules can be assumed followed by an equilibrium reaction mechanism for the adsorption of the remaining $D_2O$ molecules, according to

$$Mn_4O_4^+ + 4D_2O \rightarrow Mn_4O_4(D_2O)_4^+ \quad (1a)$$

$$Mn_4O_4(D_2O)_4^+ + D_2O \rightleftarrows Mn_4O_4(D_2O)_5^+ \quad (1b)$$

$$Mn_4O_4(D_2O)_5^+ + D_2O \rightleftarrows Mn_4O_4(D_2O)_6^+ \quad (1c)$$

This indicates the strong nonreversible and potentially activated adsorption of the first four water molecules and weaker molecular binding of the fifth and sixth water molecules.

**B. $^{18}O$-Exchange Reaction.** To elucidate the potential water activation and deprotonation capability of the tetra-manganese oxide cluster, $Mn_4O_4^+$, as well as the role of the cluster oxygen atoms in this process, the ion trap reaction

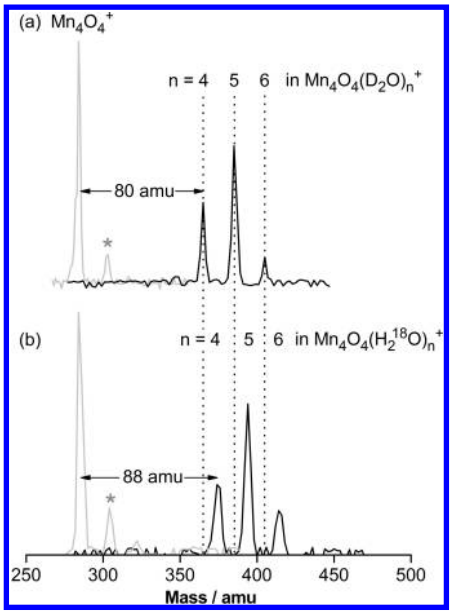


**Figure 1.** Mass spectra obtained before (light gray signals) and after (black signals) the reaction of $Mn_4O_4^+$ with (a) $D_2O$ and (b) $H_2{}^{18}O$ (reaction time $t_R$ = 0.1 s). *n* indicates the number of adsorbed water molecules in $Mn_4O_4(D_2O)_{4,5,6}^+$ and $Mn_4O_4(H_2{}^{18}O)_{4,5,6}^+$, respectively. Peaks labeled with an asterisk correspond to $Mn_4O_4(H_2{}^{16}O)^+$ and originate from the reaction of $Mn_4O_4^+$ with residual trace amounts of $H_2{}^{16}O$.

experiments have been repeated with $H_2{}^{18}O$. In the case of simple molecular water adsorption the product mass spectrum should, at equal experimental conditions, be identical to the one displayed in Figure 1a because $D_2O$ and $H_2{}^{18}O$ have the same mass (20 amu).

A typical mass spectrum obtained after the reaction of $Mn_4O_4^+$ with $H_2{}^{18}O$ is displayed in Figure 1b (black line). It exhibits three peaks with an intensity distribution similar to that obtained for the reaction with $D_2O$ in Figure 1a. However, these peaks are shifted by 88, 108, and 128 amu from the position of the unreacted cluster signal (gray line) in the mass spectrum. The shift of the complete product mass spectrum by 8 amu compared to the mass spectrum obtained with $D_2O$ can be explained only by an exchange of the four $^{16}O$ atoms of the $Mn_4O_4^+$ cluster by $^{18}O$ atoms originating from $H_2{}^{18}O$. Thus, the observed ion signals correspond to the complexes $Mn_4{}^{18}O_4(H_2{}^{18}O)_4^+$, $Mn_4{}^{18}O_4(H_2{}^{18}O)_5^+$, and $Mn_4{}^{18}O_4(H_2{}^{18}O)_6^+$ with $Mn_4{}^{18}O_4(H_2{}^{18}O)_5^+$ as the most intense signal.

Furthermore, the ion trap reactivity experiment allows for the determination of rate constants by recording the intensity of the bare cluster signal as well as that of the observed reaction intermediates and final products as a function of the reaction time, i.e., the storage time inside the ion trap. However, as mentioned previously, in the present case the separate reactions of $D_2O$ and $H_2{}^{18}O$ with $Mn_4O_4^+$ as well as the $^{16}O/^{18}O$ exchange are faster than the shortest possible ion trap storage time in the current experiment (about 0.1 s). Thus, a lower limit for the overall reaction rate constant can be estimated: $k \geq 10\ s^{-1}$. This pseudo first-order rate constant includes the reaction of $Mn_4O_4^+$ with five water molecules, the exchange of all four oxygen atoms $^{16}O$ of $Mn_4{}^{16}O_4^+$ with four water $^{18}O$ atoms, as well as the subsequent displacement of the formed $H_2{}^{16}O$ molecules by $H_2{}^{18}O$.



DOI: 10.1021/jp5106532
J. Phys. Chem. C 2015, 119, 10881−10887

**C. Water Deprotonation via Oxo-Bridge Hydroxylation.** Recent detailed SDFT calculations by some of the present authors revealed a two-dimensional (2D) ring structure containing $\mu_2$-oxo-bridges between each two manganese atoms as the lowest-energy geometry of the bare $Mn_4O_4^+$ cluster.[19] However, already upon adsorption of only two water molecules a dimensionality crossover occurs and the 2D ring geometry of $Mn_4O_4^+$ is transformed into a three-dimensional cubic $Mn_4O_4^+$ core with $H_2O$ bound to the Mn atom vertices via the water oxygen atoms. The calculated structure of the complex $Mn_4O_4(H_2O)_4^+$ with four adsorbed water molecules is depicted in Figure 2 (structure **A**).

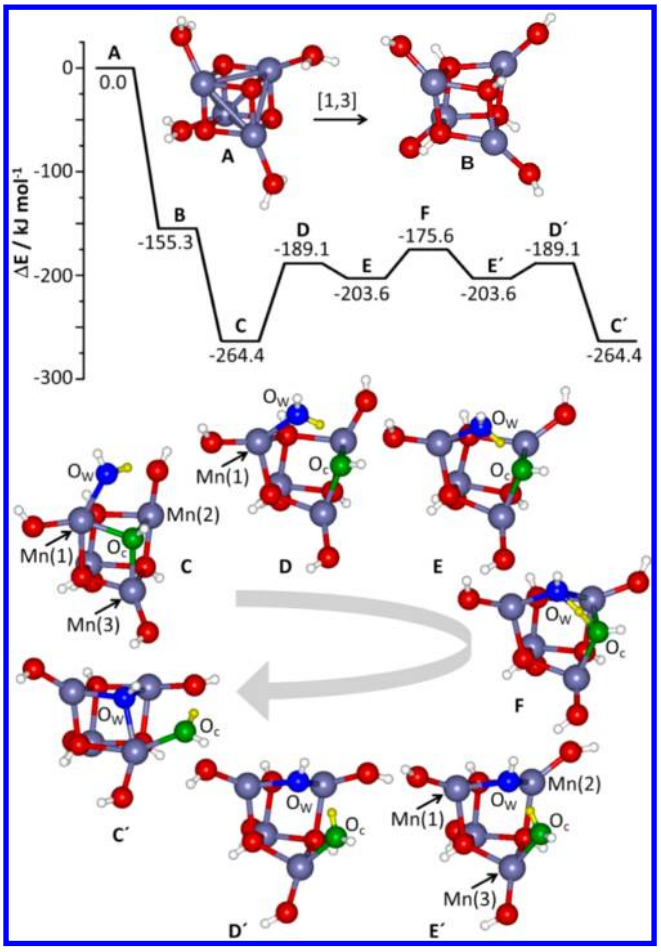


**Figure 2.** Calculated reaction pathway for water deprotonation via $\mu_3$-oxo-bridge hydroxylation at $Mn_4O_4^+$ to form the octa-hydroxy complex $Mn_4(OH)_8^+$ (**A** → **B**) as well as for the subsequent $\mu_3$-oxo-bridge exchange (**C** → **D** → **E** → **F** → **E′** → **D′** → **C′**). Manganese, oxygen, and hydrogen atoms are depicted as purple, red, and white spheres, respectively. For the sake of clarity, the exchanging oxygen atoms of the water molecule, $O_w$, and of the cluster complex, $O_c$, are highlighted in blue and green, respectively. The hydrogen atom transferred from $H_2O_w$ to the hydroxyl-group $O_cH$ of the complex is colored in yellow. The Cartesian coordinates of all the atoms in configurations **A**–**F** (with **F** being the configuration at the top of the activation energy barrier) are given in the Supporting Information, together with information about the Mn–Mn and Mn–O distances and oxidation states of the individual Mn and O atoms throughout the exchange reaction. The spin projection ($S_z$ = 19/2) remains the same throughout the entire water exchange reaction; for the properties of some higher-energy spin isomers at different stages of the reaction (e.g., $S_z$ = 9/2 and 1/2), see the Supporting Information.

Furthermore, the change in dimensionality was predicted to facilitate the activation of one O–H bond in each water molecule in this complex leading to a subsequent hydrogen atom migration to a $\mu_3$-oxo-bridge of the cuboidal tetra-manganese oxide cluster via a [1,3] shift to form an octa-hydroxy complex $Mn_4(OH)_8^+$ (cf. structure **B** in Figure 2). This intramolecular dehydration reaction[29] was found to be virtually activation-barrier-free (the calculated energy barriers are smaller than 5 kJ/mol) and exothermic by 155.3 kJ/mol (i.e., 38.8 kJ/mol for each formed O–H bond).[19] In contrast, the alternative [1,2] shift of the hydrogen atom to the Mn atom would be endothermic as also evidenced by thermodynamic data for the manganese cation.[30]

Additional water molecules were predicted to bind molecularly to the octa-hydroxy complex. These theoretical findings are in excellent agreement with the experimental observation of the nonreversible, potentially activated adsorption of the first four water molecules (reaction 1a) and the reversible, molecular binding of the fifth and sixth water molecules (reactions 1b and 1c, respecitvely).

The importance of the hydroxylation of an exchanging $\mu_3$-oxo-bridge as the first reaction step in the oxygen evolution reaction has recently also been demonstrated by SDFT calculations on models for the $S_1$, $S_2$, and $S_3$ states of the Kok cycle in the biological photosystem II.[7] Furthermore, hydrogen migration via a [1,3] shift has been proposed by Brudvig and co-workers[31] as the initial reaction step for $^{16}O/^{18}O$-exchange in $[Mn_2(\mu\text{-}O)_2]^{3+}$ based on experimental data and also by Siegbahn and co-workers[32] in a theoretically predicted exchange mechanism for $[Mn_2(\mu\text{-}O)_2]^{4+}$. Predicated on the absence of an H/D isotope effect, this protonation step was experimentally found not to be rate-determining in the condensed phase model complex system; instead, it appears to be fast on the time scale of the exchange reaction.[31] This finding is also in full agreement with our theoretical studies which reveal an almost activation-barrier-free hydroxylation reaction.[19]

**D. Mechanism of the $\mu_3$-Oxo-Bridge Exchange.** To gain molecular level insight into the experimentally observed $^{16}O/^{18}O$ exchange mechanism, first-principles SDFT calculations have been performed. Starting from the octa-hydroxy complex $Mn_4(OH)_8^+$ (structure **B** in Figure 2), the first reaction step represents the adsorption of a fifth water molecule (adsorption energy $E_a$ = 109.0 kJ/mol) which binds molecularly via coordination of the oxygen atom (labeled $O_w$ in Figure 2 and highlighted by blue coloring) to the Mn(1) atom (structure **C**). The subsequent exchange of a $\mu_3$-bridge oxygen atom $O_c$ of the cluster complex (indicated by green coloring) by $O_w$ involves three steps: (1) the activation and breaking of an Mn(1)—$O_c$ bond and thus the opening of the cuboidal $Mn_4O_4^+$ structure (**C** → **D** → **E**, energy barrier $\Delta E_b$ = 75.3 kJ/mol); (2) the transfer of a hydrogen atom (indicated by yellow coloring) from $O_w$ to $O_c$ in conjunction with the formation of a new oxo-bridge Mn(1)—$O_w$—Mn(2) as well as the breaking of a second oxo-bridge Mn(2)—$O_c$—Mn(3) to form a new adsorbed water molecule $H_2O_c$ (**E** → **F** ($d_{O_w-H} = d_{H-O_c}$ = 1.21 Å) → **E′** ($d_{O_w-H}$ = 1.61 Å; $d_{H-O_c}$ = 1.02 Å); $\Delta E_b$ = 28.0 kJ/mol); and (3) the final formation of the Mn(3)—$O_w$ bond which results in the closing of the cuboidal $Mn_4O_4^+$ structure (**E′** → **D′** ($d_{O_w-H}$ = 1.95 Å; *d*H–Oc = 0.99 Å) → **C′** ($d_{O_w-H}$ = 2.85 Å; $d_{H-O_c}$ = 1.04 Å); $\Delta E_b$ = 14.5 kJ/mol). For further



DOI: 10.1021/jp5106532
J. Phys. Chem. C 2015, 119, 10881–10887

details about the geometrical characterization of the atomic configurations involved in the exchange reaction, as well as information about the atomic oxidation states and higher-energy spin state isomers, see the Supporting Information.

The final release of the thus formed $H_2O_c$ molecule (with the $O_c$ oxygen atom colored green in structure **C′**) entails an energy barrier of 109.0 kJ/mol, which is, of course, equivalent to the initial adsorption energy of $H_2O_w$. In the experiment, an equilibrium reaction mechanism has been observed for the adsorption of the fifth water molecule (reaction 1b), and the mass spectrum in Figure 1b does exhibit only $^{18}O$-exchanged product complexes ($Mn_4{}^{18}O_4(H_2{}^{18}O)_4^+$, $Mn_4{}^{18}O_4(H_2{}^{18}O)_5^+$, and $Mn_4{}^{18}O_4(H_2{}^{18}O)_6^+$), thus confirming the facile release and displacement of the exchanged water molecule under the experimental conditions.

Calculations were also performed for the neutral $Mn_4(OH)_8$ complex and yielded the identical mechanism with similar energy barriers, thus demonstrating that the positive charge of the gas-phase cluster has no crucial influence on the mechanistic and energetic details.

**E. Rate Constants of the $^{18}O$-Exchange and Implications for the $O_2$ Evolution Mechanism in Photosystem II.** In the natural photosystem II the $^{18}O$-exchange rate constants of the two substrate water molecules that are required for the formation of molecular oxygen at the OEC differ quite significantly, as evidenced by time-resolved membrane inlet mass spectrometry.[8−11] The rate constant of the faster oxygen exchange ranges between 40 $s^{-1}$ and more than 120 $s^{-1}$ (this oxygen atom is assigned to a terminal oxygen atom in the OEC[11]), whereas the rate constant of the more slowly exchanging oxygen amounts to 0.02−10 $s^{-1}$ depending on the oxidation state of the Mn atoms in the different $S_n$ states.

Most interestingly, on the basis of the most recent crystal structure of the OEC,[2] $S_n$ state-dependent $^{18}O$-exchange experiments,[10] Ca/Sr substitution,[12] as well as NMR spectroscopic data,[13] the slowly exchanging substrate water has been assigned to provide the oxygen that replaces a $\mu_3$-oxo-bridge located at one corner of the $Mn_3CaO_4$ cube of the OEC and that additionally bridges the dangling fourth Mn atom.[11]

This assignment is, however, in contradiction to $^{18}O$-exchange reaction rates obtained for oxo-bridges in solvated ligand-stabilized manganese oxide model complexes. The rate constants for the exchange of doubly coordinated oxygen in bimanganese oxo-complexes $[Mn_2(\mu\text{-}O)_2]^{2+}$, $[Mn_2(\mu\text{-}O)_2]^{3+}$, and $[Mn_2(\mu\text{-}O)_2]^{4+}$ are orders of magnitude below the slow $^{18}O$-exchange rate constants in the OEC and range between $10^{-3}$ and $10^{-5}$ $s^{-1}$ depending on the experimental conditions,[33,34] whereas the rate constants for the 3-fold coordinated oxygen in tetra-manganese oxo-complexes are even smaller. Ohlin et al. experimentally determined rate constants of $10^{-5}$−$10^{-6}$ $s^{-1}$ for the exchange of 3-fold coordinated $\mu_3$-oxygen atoms in $[Mn_4O_4]^{6+}$.[35] Even more remarkably, Tagore et al.[33] and Kanady et al.[18] have not observed any exchange reaction for $[Mn_4O_4]^{6+}$, $[Mn_4O_5]^{6+}$, and $[Mn_4O_6]^{4+}$.

In marked contrast, the present data, obtained through the use of gas-phase isolated $Mn_4O_4(H_2O)_n^+$ clusters, provide for the first time experimental evidence for oxygen exchange rates in manganese-oxide model complexes that are well in agreement with those obtained for the slower exchanging water in the OEC of photosystem II. In the following we compare our results to the OEC exchange reaction in more detail and discuss the discrepancies in relation to the exchange rates obtained with ligated manganese oxide complexes.

The rate constant of ≥10 $s^{-1}$ determined in our gas-phase study includes several reaction steps such as the adsorption of five water molecules, the exchange of all four $\mu_3$-oxo-bridges, and the desorption or replacement of the final exchanged water molecules. The molecular details of these reactions have been revealed through our SDFT calculations, as shown in Figure 2. The calculated structures demonstrate the cuboidal geometry of the cluster complexes $Mn_4O_4(H_2O)_4^+$ and $Mn_4O_4(H_2O)_5^+$. Thus, the oxygen exchange in these clusters indeed involves oxygen atoms bound to three metal centers (Mn(1), Mn(2), and Mn(3) in Figure 2), very similar to the proposed process in the OEC.[11]

Furthermore, the estimated activation barrier for oxo-bridge exchange in the free $Mn_4O_4^+$ amounts to 88.4 kJ/mol (energy difference between structure **C** and the activation barrier configuration **F** in Figure 2). This is in most favorable agreement with experimentally determined activation energies for the substrate water exchange in the $S_1$ (83 ± 4 kJ $mol^{-1}$), $S_2$ (71 ± 9 kJ $mol^{-1}$), and $S_3$ states (78 ± 9 kJ $mol^{-1}$)[11] as well as with theoretically predicted activation barriers in the $S_1$ (91 kJ $mol^{-1}$) and $S_2$ state (74 kJ $mol^{-1}$) of the OEC in the biological photosystem II.[7]

The calculated activation energy (88.4 kJ/mol) for the oxo-bridge exchange in $Mn_4O_4^+$ can now be used to determine the rate constant for this reaction. For this purpose statistical rate theory on the basis of the Rice, Ramsperger, Kassel, and Marcus (RRKM) formalism[36−38] has been employed. This results in a rate constant of about 6 $s^{-1}$ for the $\mu_3$-oxo-bridge exchange in $Mn_4(OH)_8(H_2O)^+$, which is in excellent accord with the experimentally determined lower limit of the rate constant of 10 $s^{-1}$ and also with the $^{18}O$-exchange rate constants measured for the OEC in the states $S_0$ (10 $s^{-1}$), $S_2$ (2.0 $s^{-1}$), and $S_3$ (2.0 $s^{-1}$);[11] the rate constant measured for the OEC in state $S_1$ is found to be smaller (0.02 $s^{-1}$).[11]

Nevertheless, all of these rate constants for $\mu$-oxo-bridge exchange reactions are orders of magnitude larger than those determined for the solvated di- and tetra-manganese model complexes, as mentioned above.[18,33−35] While the reason for this discrepancy remains largely elusive, it is pertinent to consider in this context two additional observations.

First, investigations with terminal and bridging water exchange in inorganic manganese oxide model complexes showed that the exchange rate constants increase as the oxidation state of the Mn atoms decreases;[33,34,39] for the calculated oxidation states of the individual Mn atoms in the $Mn_4O_4(H_2O)_5^+$ cluster throughout the process leading to the top of the activation energy barrier of the water exchange reaction, see the Supporting Information. This observation might hint toward an explanation why the exchange rate constants measured here for the free cluster complexes (lower limit of 10 $s^{-1}$) might even be larger than those in the biological OEC. The Mn atom formal oxidation state in the free $Mn_4(OH)_8^+$ cluster ranges between II and III and is thus lower than that for the Mn atoms of the OEC, which typically exhibits Mn atom oxidation states between III and IV depending on the $S_n$ state.[11]

Second, it has been noted that water exchange rates in metal ion aqua-complexes increase as the hydration level is increased.[39] Thus, the additional water observed here in the detected complexes $Mn_4O_4(H_2O)_5^+$ and $Mn_4O_4(H_2O)_6^+$ might support the facile oxygen exchange. Similar effects have been


DOI: 10.1021/jp5106532
J. Phys. Chem. C 2015, 119, 10881−10887

reported for dimanganese oxo-complexes, in which the oxo-exchange rates are enhanced if terminal water molecules are bound to the Mn ion.[33]

## IV. CONCLUSION

The reported findings suggest that with obvious relative simplification, the free $Mn_4O_4^+$−water complexes synthesized in an ion trap gas-phase experiment bring forth suitable model systems for the OEC of the biological photosystem II. As mentioned previously, the first-principles SDFT calculations reveal that the detected cluster complexes $Mn_4O_4(H_2O)_n^+$ ($n$ = 4−6) exhibit a cuboidal structure which is very similar to the OEC inorganic core geometry. Furthermore, nearly barrier-free $\mu$-oxo-bridge hydroxylation via [1,3] hydrogen shift has been predicted theoretically. The subsequent $\mu_3$-oxo-bridge exchange by additional water has been evidenced experimentally by $^{18}O/^{16}O$-exchange studies. The estimated rate constant for the oxo-bridge exchange in the tetra-manganese oxide complexes agrees well with $^{18}O$-exchange rate constants determined for the OEC of photosystem II in the different oxidation states of the Kok cycle. Finally, the experimentally found lower oxo-bridge exchange rate constant limit of 10 $s^{-1}$ is in most satisfactory agreement with the rate constant derived from the theoretically estimated activation barriers of the detailed molecular oxygen exchange mechanism as obtained by our SDFT study.

The present contribution successfully demonstrates a new hierarchical approach employing the synthesis and investigation of simplified but nevertheless meaningful model systems for the biological OEC of photosystem II, which are able to provide molecular level insight into the details of water activation and oxygen evolution mechanism. We remark here that preliminary theoretical explorations in our laboratories indicate the possibility of O−O bond formation upon the interaction of water molecules with gas-phase $Mn_3CaO_4^+$, resulting in ejection of $H_2O_2$, that is $2H_2O(a) \rightarrow H_2O_2(g) + 2H(a)$ where (a) and (g) denote adsorbed and gaseous species, respectively; notably, this reaction does not occur on the tetra-manganese oxide cluster. Concurrent experimental work on the interaction of water with a calcium manganese oxide cluster is currently in progress.[40] Future efforts in our laboratories pertaining to the first step of this hierarchical approach will be directed toward the improvement of the time resolution of the ion trap experiments and spectroscopic characterization (including vibrational spectroscopy) of the gas-phase cluster complexes.[19] Further hierarchical steps will focus on distinct tailoring of the oxidation states of the manganese centers through the addition of appropriate ligands to the gas-phase cluster complexes.

## ■ ASSOCIATED CONTENT

### Supporting Information

Spin configurations, Bader charge analysis, and coordinates of structural configurations along the reaction path. This material is available free of charge via the Internet at http://pubs.acs.org.

## ■ AUTHOR INFORMATION

### Corresponding Authors

*Phone: +49-731-50-25455. E-mail: thorsten.bernhardt@uni-ulm.de.
*Phone: +1-404-894-7747. E-mail: uzi.landman@physics.gatech.edu.

### Notes

The authors declare no competing financial interest.

## ■ ACKNOWLEDGMENTS

S.M.L. is grateful to the ESF Baden-Württemberg for a Margarete von Wrangell fellowship. The work of R.N.B. at the Georgia Institute of Technology was supported by a grant from the U.S. Air Force Office of Scientific Research, and the work of U.L. was supported in part by a grant from the Office of Basic Energy Sciences of the U.S. Department of Energy under Contract FG05-86ER45234. Calculations were performed at the Georgia Institute of Technology Center for Computational Materials Science.

## ■ REFERENCES

(1) *Photosystem II The Light-Driven Water: Plastoquinone Oxidoreductase*; Wydrzynski, T. J.; Sato, K., Eds.; Springer: Dordrecht, 2005.
(2) Umena, Y.; Kawakami, K.; Shen, J.-R.; Kamiya, N. Crystal Structure of Oxygen-Evolving Photosystem II at a Resolution of 1.9 Å. *Nature* **2011**, *473*, 55−60.
(3) McEvoy, J. P.; Brudvig, G. W. Water-Splitting Chemistry of Photosystem II. *Chem. Rev. (Washington, DC, U.S.)* **2006**, *106*, 4455−4483.
(4) Dau, H.; Limberg, C.; Reier, T.; Risch, M.; Roggan, S.; Strasser, P. The Mechanism of Water Oxidation: From Electrolysis via Homogeneous to Biological Catalysis. *ChemCatChem* **2010**, *2*, 724−761.
(5) Dau, H.; Zaharieva, I.; Haumann, M. Recent Developments in Research on Water Oxidation by Photosystem II. *Curr. Opin. Chem. Biol.* **2012**, *16*, 3−10.
(6) Siegbahn, P. E. M. Structures and Energetics for $O_2$ Formation in Photosystem II. *Acc. Chem. Res.* **2009**, *42*, 1871.
(7) Siegbahn, P. E. M. Substrate Water Exchange for the Oxygen Evolving Complex in PSII in the $S_1$, $S_2$, and $S_3$ States. *J. Am. Chem. Soc.* **2013**, *135*, 9442−9449.
(8) Messinger, J.; Badger, M.; Wydrzynski, T. Detection of One Slowly Exchanging Substrate Water Molecule in the $S_3$ State of Photosystem II. *Proc. Nat. Acad. Sci. U.S.A.* **1995**, *92*, 3209−3213.
(9) Hillier, W.; Messinger, J.; Wydrzynski, T. Kinetic Determination of the Fast Exchanging Substrate Water Molecule in the $S_3$ State of Photosystem II. *Biochemistry* **1998**, *37*, 16908−16914.
(10) Hillier, W.; Wydrzynski, T. The Affinities for the Two Substrate Water Binding Sites in the $O_2$ Evolving Complex of Photosystem II Vary Independently during S-State Turnover. *Biochemistry* **2000**, *39*, 4399−4405.
(11) Cox, N.; Messinger, J. Reflections on Substrate Water and Dioxygen Formation. *Biochim. Biophys. Acta* **2013**, *1827*, 1020−1030.
(12) Hendry, G.; Wydrzynski, T. $^{18}O$ Isotope Exchange Measurements Reveal that Calcium Is Involved in the Binding of One Substrate-Water Molecule to the Oxygen-Evolving Complex in Photosystem II. *Biochemistry* **2003**, *42*, 6209−6217.
(13) Rapatskiy, L.; Cox, N.; Savitsky, A.; Ames, W. M.; Sander, J.; Nowaczyk, M. M.; Rögner, M.; Bourssac, A.; Neese, F.; Messinger, J.; Lubitz, W. Detection of the Water-Binding Sites of the Oxygen-Evolving Complex of Photosystem II Using W-Band $^{17}O$ Electron−Electron Double Resonance-Detected NMR Spectroscopy. *J. Am. Chem. Soc.* **2012**, *134*, 16619.
(14) Yagi, M.; Kaneko, M. Molecular Catalysts for Water Oxidation. *Chem. Rev. (Washington, DC, U.S.)* **2001**, *101*, 21−36.
(15) Rüttinger, W.; Dismukes, G. C. Synthetic Water-Oxidation Catalysts for Artificial Photosynthetic Water Oxidation. *Chem. Rev. (Washington, DC, U.S.)* **1997**, *97*, 1−24.
(16) Mukhopadhyay, S.; Mandal, S. K.; Bhaduri, S.; Armstrong, W. H. Manganese Clusters with Relevance to Photosystem II. *Chem. Rev. (Washington, DC, U.S.)* **2004**, *104*, 3981−4026.
(17) Dismukes, G. C.; Brimblecombe, R.; Felton, G. A. N.; Pryadun, R. S.; Sheats, J. E.; Spiccia, L.; Swiegers, G. F. Development of




DOI: 10.1021/jp5106532
J. Phys. Chem. C 2015, 119, 10881−10887

Bioinspired $Mn_4O_4$-Cubane Water Oxidation Catalysts: Lessons from Photosynthesis. *Acc. Chem. Res.* **2009**, *42*, 1935−1943.
(18) Kanady, J. S.; Mendoza-Cortes, J. L.; Tsui, E. Y.; Nielsen, R. J.; Goddard, W. A., III; Agapie, T. Oxygen Atom Transfer and Oxidative Water Incorporation in Cuboidal $Mn_3MO_n$ Complexes Based on Synthetic, Isotopic Labeling, and Computational Studies. *J. Am. Chem. Soc.* **2013**, *135*, 1073−1082.
(19) Lang, S. M.; Fleischer, I.; Bernhardt, T. M.; Barnett, R. N.; Landman, U. Dimensionality Dependent Water Splitting Mechanisms on Free Manganese Oxide Clusters. *Nano Lett.* **2013**, *13*, 5549−5555.
(20) Kok, B.; Forbush, B.; McGloin, M. Cooperation of Charges in Photosynthetic $O_2$ Evolution—I. A Linear Four Step Mechanism. *Photochem. Photobiol.* **1970**, *11*, 457−475.
(21) Bernhardt, T. M. Gas Phase Reaction Kinetics of Small Gold and Silver Clusters. *Int. J. Mass Spectrom.* **2005**, *243*, 1−29.
(22) Barnett, R. N.; Landman, U. Born-Oppenheimer Molecular Dynamics Simulations of Finite Systems: Structure and Dynamics of $(H_2O)_2$. *Phys. Rev. B: Condens. Matter Mater. Phys.* **1993**, *48*, 2081−2097.
(23) Troullier, N.; Martins, J. L. Efficient Pseudopotentials for Plane-Wave Calculations. *Phys. Rev. B: Condens. Matter Mater. Phys.* **1991**, *43*, 1993−2006.
(24) Perdew, J. P.; Burke, K.; Ernzerhof, M. Generalized Gradient Approximation Made Simple. *Phys. Rev. Lett.* **1996**, *77*, 3865−3868.
(25) Luber, S.; Rivalta, I.; Umena, Y.; Kawakami, K.; Shen, J.-R.; Kamiya, N.; Brudvig, G. W.; Batista, V. S. $S_1$-State Model of the $O_2$-Evolving Complex of Photosystem II. *Biochemistry* **2011**, *50*, 6308−6311.
(26) Ames, W.; Pantazis, D. A.; Krewald, V.; Cox, N.; Messinger, J.; Lubitz, W.; Neese, F. Theoretical Evaluation of Structural Models of the $S_2$ State in the Oxygen Evolving Complex of Photosystem II: Protonation States and Magnetic Interaction. *J. Am. Chem. Soc.* **2011**, *133*, 19743−19757.
(27) Kurashige, Y.; Chan, G. K.-L.; Yanai, T. Entangled Quantum Electronic Wavefunctions of the $Mn_4CaO_5$ Cluster in Photosystem II. *Nat. Chem.* **2013**, *5*, 660−666.
(28) Bernhardt, T. M.; Heiz, U.; Landman, U. Chemical and Catalytic Properties of Size-Selected Free and Deposited Clusters. In *Nanocatalysis*; Heiz, U., Landman, U., Eds.; Springer-Verlag: Berlin, 2007; pp 1−191.
(29) Brönstrup, M.; Schröder, D.; Schwarz, H. Reactions of Bare $FeO^+$ with Element Hydrides $EH_n$ (E = C, N, O, F, Si, P, S, Cl). *Chem.—Eur. J.* **1999**, *5*, 1176−1185.
(30) Magnera, T. F.; David, D. E.; Michl, J. Gas-Phase Water and Hydroxyl Binding Energies for Monopositive First-Row Transition-Metal Ions. *J. Am. Chem. Soc.* **1989**, *111*, 4100−4103.
(31) Tagore, R.; Crabtree, R. H.; Brudvig, G. W. Distinct Mechanisms of Bridging-Oxo Exchange in Di-$\mu$-O Dimanganese Complexes with and without Water-Binding Sites: Implications for Water Binding in the $O_2$-Evolving Complex of Photosystem II. *Inorg. Chem.* **2007**, *46*, 2193−2203.
(32) Lundberg, M.; Blomberg, M. R. A.; Siegbahn, P. E. M. Modeling Water Exchange on Monomeric and Dimeric Mn Centers. *Theor. Chem. Acc.* **2003**, *110*, 130−143.
(33) Tagore, R.; Chen, H.; Crabtree, R. H.; Brudvig, G. W. Determination of $\mu$-Oxo Exchange Rates in Di-$\mu$-Oxo Dimanganese Complexes by Electrospray Ionization Mass Spectrometry. *J. Am. Chem. Soc.* **2006**, *128*, 9457−9465.
(34) Dubois, L.; Pécaut, J.; Charlot, M.-F.; Baffert, C.; Collomb, M.-N.; Deronzier, A.; Latour, J.-M. Carboxylate Ligands Drastically Enhance the Rates of Oxo Exchange and Hydrogen Peroxide Disproportionation by Oxo Manganese Compounds of Potential Biological Significance. *Chem.—Eur. J.* **2008**, *14*, 3013−3025.
(35) Ohlin, C. A.; Brimblecombe, R.; Spiccia, L.; Casey, W. H. Oxygen Isotopic Exchange in an $Mn^{III}Mn_3^{IV}$-Oxo Cubane. *Dalton Trans.* **2009**, 5278−5280.
(36) Marcus, R. A. Unimolecular Dissociations and Free Radical Recombination Reactions. *J. Chem. Phys.* **1952**, *20*, 359−364.
(37) Holbrook, K. A.; Pilling, M. J.; Robertson, S. H. *Unimolecular Reactions*, 2nd ed.; John Wiley & Sons Ltd.: Chichester, U.K., 1996.
(38) Bernhardt, T. M.; Hagen, J.; Lang, S. M.; Popolan, D. M.; Socaciu-Siebert, L.; Wöste, L. Binding Energies of $O_2$ and CO to Small Gold, Silver, and Binary Silver-Gold Cluster Anions from Temperature Dependent Reaction Kinetics Measurements. *J. Phys. Chem. A* **2009**, *113*, 2724−2733.
(39) Hillier, W.; Wydrzynski, T. $^{18}O$-Water Exchange in Photosystem II: Substrate Binding and Intermediates of the Water Splitting Cycle. *Coord. Chem. Rev.* **2008**, *252*, 306−317.
(40) Lang, S. M.; Fleischer, I.; Bernhardt, T. M.; Barnett, R. N.; Landman, U. to be published.




DOI: 10.1021/jp5106532
*J. Phys. Chem. C* 2015, 119, 10881−10887